MAXIMISING GEOLOGICAL INFORMATION RECOVERY FROM DIFFERENT MAGNETIC INSTRUMENTS THROUGH THE APPLICATION OF JOINT INVERSION

David Pratt, David.Pratt@encom.com.au and K. Blair McKenzie, Blair.McKenzie@encom.com.au
Encom Technology, Sydney, Australia

Key Words: inversion, joint, tensor, gradiometer, magnetic, gravity.

INTRODUCTION

Magnetic instruments such as cross-wing gradiometers, vertical gradiometers and full tensor SQUID magnetometers presented challenges for geological interpretation and geophysical inversion. In particular, the full tensor magnetometer presents many new challenges for an interpreter where only the vertical derivative of the vertical magnetic component presents a useful geological analogue for visual interpretation. With six channels of information how do we make practical use of the other five channels which implicitly contain useful information about the 3D distribution of magnetic properties?

Joint inversion of all six channels is the logical solution whereby the data is inverted directly to a 3D magnetic susceptibility model. When compared with the scalar amplitude of the total magnetic intensity measurement, the magnetic tensor has valuable 3D information. For example just a few samples can provide sufficient information to immediately determine if an igneous pipe is on the left or right side of the flight line. A few more samples can locate the position and depth of a pipe that is off to the side of a flight line.

Joint inversion can be used with various combinations of sensors and derived parameters. For example a cross-wing total magnetic field gradiometer can be used with the centre point total field value to derive important off-line geological information. The first vertical derivative derived from gridded data can be combined with total magnetic intensity measurements for two channel joint inversion to optimise the quality of depth, width, dip and depth extent inversions.

Examples are provided to illustrate the improvement in geological information extraction when compared with single channel inversion of total magnetic intensity data. The methods provide new opportunities to look at the latest generation of instruments and new ways to look at old surveys.

THEORETICAL BACKGROUND

Our current implementation of joint inversion limits the problem to cover measurements from multiple sensors at a series of x, y, z locations where all data channels are available at each location. The algorithm does not presently support simultaneous inversion for multiple physical properties, although this can be done cooperatively by using the same model sequentially. The following section provides a brief overview of the theory behind our joint inversion algorithm development.

In the context of this paper, the joint inversion of multi-channel magnetic or gravity data is a constrained, cooperative, parametric non-linear inversion of fully overlapping data sets $\mathbf{d}_{obs} = (\mathbf{d}_1, \mathbf{d}_2, \ldots, \mathbf{d}_{Nchan})^T$ gathered simultaneously at N_s observation points $\mathbf{r}_1, \mathbf{r}_2, \ldots, \mathbf{r}_{Ns}$. Each channel (j) contains N_s data points so that $\mathbf{d}_j = [d_j(\mathbf{r}_1), d_j(\mathbf{r}_2), \ldots, d_j(\mathbf{r}_{Ns})]^T$. Hence for all

the N_{chan} data channels there are a total of $N_d = N_s N_{chan}$ data observations, i.e. $\mathbf{d_{obs}} = \{\mathbf{d_j}\}$ $[j=1: N_{chan}] = \mathbf{d_1} \cup \mathbf{d_2} \cup \mathbf{d_3} \cup \ldots \cup \mathbf{d_j} \cup \ldots \cup \mathbf{d_{Nchan}}$.

From a statistical viewpoint, the set of N_d data observations $\mathbf{d}_{obs}[1:N_d]$ are considered to be incomplete and insufficient with standard errors $\sigma_d[1:N_d]$. Whence the non-linear inverse problem may be stated as follows: given a forward modelling function $\boldsymbol{f}(\mathbf{m};\{\mathbf{r_i}\})$ containing N_p model parameters $\mathbf{m} = (m_1, m_2, \ldots, m_{Np})^T$, then find an optimum solution vector $\mathbf{m}_{best}$ such that the total standardised residual squared error $Q_d = ||\mathbf{e_d}||^2 = \mathbf{e_d}^T \cdot \mathbf{e_d}$ between the set of N_d observed data observations $\mathbf{d_{obs}}[1:N_d]$ and the set of N_d predicted or modelled data observations $\mathbf{d_{mod}}[1:N_d] = \boldsymbol{f}(\mathbf{m};\{\mathbf{r_i}\})$ $[1:N_d]$ is minimised subject to some constraints on the physical reliability of the model parameters themselves. In this instance the objective function or functional $Q_t(\mathbf{m})$ to be minimised is:

$$Q_t(\mathbf{m}) = Q_d(\mathbf{m}) + \mu Q_m(\mathbf{m}) = [\mathbf{e_d}^T \cdot \mathbf{e_d}] + \mu [\mathbf{e_m}^T \mathbf{e_m}] = ||\mathbf{e_d}||^2 + \mu ||\mathbf{e_m}||^2 \qquad (1)$$

where $Q_d(\mathbf{m}) = ||\mathbf{e_d}||^2$ is the measure of the data misfit (the L_2 norm); $Q_m(\mathbf{m}) = ||\mathbf{e_m}||^2$ is a measure of the relative change in the model parameters and $\mu > 0$ is a Lagrange multiplier. The objective function Q_t may be further expressed as:

$$Q_t(\mathbf{m}) = [(\mathbf{d_{obs}} - \boldsymbol{f}(\mathbf{m};\{\mathbf{r_i}\})/\boldsymbol{\sigma_d}]^T [(\mathbf{d_{obs}} - \boldsymbol{f}(\mathbf{m};\{\mathbf{r_i}\}))/\boldsymbol{\sigma_d}] + \mu [\mathbf{x_s}^T \mathbf{x_s} - R_0^2] \qquad (2)$$

where $\mathbf{y} = \mathbf{e_d} = [\mathbf{d_{obs}} - \boldsymbol{f}(\mathbf{m};\{\mathbf{r_i}\})/\boldsymbol{\sigma_d}]$ is the (N_d x 1) column vector of standardised errors between the observed and modelled data measurements; $\mathbf{e_d}^T$ is the transpose of $\mathbf{e_d}$; $\mathbf{x_s} = x_{s[j]}[1: N_p]$ is the scaled parameter step length vector and R_0^2 is the maximum bound placed on the energy level $\mathbf{x_s}^T \mathbf{x_s}$ of the scaled parameter changes. The $Q_d(\mathbf{m})$ and $Q_m(\mathbf{m})$ functionals are computed as:

$$Q_d(\mathbf{m}) = \mathbf{e_d}^T \cdot \mathbf{e_d} = ||\mathbf{e_d}||^2 = ||\mathbf{y}||^2 = \sum_{i=1}^{N_d} y_i^2 = \sum_{i=1}^{N_d} [(d_{obs[i]} - d_{mod[i]})/\sigma_{d[i]}]^2 \qquad (3a)$$

and

$$Q_m(\mathbf{m}) = \mathbf{e_m}^T \cdot \mathbf{e_m} = ||\mathbf{e_m}||^2 = \sum_{j=1}^{N_p} x_{s[j]}^2 = \sum_{j=1}^{N_p} [\delta m_j / s_j]^2 \qquad (3b)$$

where s_j is the scaling factor for the j th parameter step δm_j.

Ridge regression or the Marquardt-Levinburg method provide stable method of solving the non-linear equation $\mathbf{B_{obs}} = \boldsymbol{f}(\mathbf{m}_p;\{\mathbf{r_i}\}) + \mathbf{e_d}$ for an optimum $\mathbf{m}_{best}$ such that the objective function $Q_t(\mathbf{m})$ is minimised. Ridge regression is essentially a constrained inversion method in which the step length $||\mathbf{x_s}||$ of the solution vector $\mathbf{x_s}$ is kept within physically realizable limits.

To apply the ridge regression method, we first convert this non-linear inversion problem into an approximate linear form by expanding the response or forward modelling function $\boldsymbol{f}(\mathbf{m; r_i})$ in a Taylor series about an initial starting point $\mathbf{m}^0$, namely,

$$\boldsymbol{f}(\mathbf{m}) = \boldsymbol{f}(\mathbf{m}^0) + \mathbf{A}\,\boldsymbol{\delta}\mathbf{m} + O(||\boldsymbol{\delta}\mathbf{m}||^2) \qquad (4)$$

where $\boldsymbol{\delta}\mathbf{m} = \mathbf{m} - \mathbf{m}^0$ and $\mathbf{A}$ is the Jacobian or gradient matrix of partial derivatives of $\boldsymbol{f}(\mathbf{m;r_i})$ with respect to each of the model parameters m_j ,namely, $A_{ij} = \partial f_i(\mathbf{m; r_i})/\partial m_j$. Whence it may be shown (Meju, 1994) that the objective function $Q_t(\mathbf{m})$ in equation (2) is now:

$$Q_t = Q_d + \beta^2 Q_p = [\mathbf{y} - \mathbf{A}\,\mathbf{x_s}]^T [\mathbf{y} - \mathbf{A}\,\mathbf{x_s}] + \beta^2 [\mathbf{x_s}^T \mathbf{x_s} - R_0^2] \quad (5)$$

where $\beta^2 > 0$ is the ridge parameter or Lagrange multiplier μ. The scaled least squares solution vector $\mathbf{x_s}$ is found by expanding equation (5) and then differentiating the resulting expression with respect to $\mathbf{x_s}$. Finally setting $\partial Q_t(\mathbf{m})/\partial \mathbf{x_s} = 0$, we obtain the least squares solution for the scaled model parameter perturbation $\mathbf{x_s} = \mathbf{s}\,\delta\mathbf{m}$

$$\mathbf{x_s} = (\mathbf{A}^T \mathbf{A} + \beta^2 \mathbf{I})^{-1} \cdot \mathbf{A}^T \mathbf{y} \quad (6)$$

Whence the new model $\mathbf{m}_{k+1} = \mathbf{m}_k + \delta\mathbf{m}_k$ is given by the relation:

$$\mathbf{m}_{k+1} = \mathbf{m}_k + \mathbf{s}^{-1} (\mathbf{A}^T \mathbf{A} + \beta_k^2 \mathbf{I})^{-1} \cdot \mathbf{A}^T \mathbf{y} \qquad \text{for k=0,1,2,} \quad (7)$$

where $\mathbf{s}^{-1} = \text{diag}(1/s_j)$ for j=1: N_p is a diagonal matrix of inverse scaling factors; β_k is the optimum ridge parameter for the k th trial model step $\delta\mathbf{m}_k$ and $\mathbf{m}_k$ is the vector of model parameters from the previous (k th) iteration.

One means of accurately estimating the model parameters $\mathbf{m}_{k+1}$ as well as investigating their sensitivities during the course of the inversion is via the use of singular value decomposition (SVD) of the Jacobian matrix $\mathbf{A}$ or, in the case of joint inversion, its scaled and weighted equivalent $\mathbf{A_s} = \mathbf{W}\,\mathbf{A}\,\mathbf{s}^{-1}$ (for $\mathbf{W} = 1/\boldsymbol{\sigma_d} = \text{diag}[1/\sigma_{d[i]}]$; i=1:N_d]). For example, the singular value decomposition of the (N_d x N_p) matrix $\mathbf{A_s}$ is [see Menke, 1989; Press *et al*, 1993]

$$\mathbf{A_s} = \mathbf{U}\,\boldsymbol{\lambda}\,\mathbf{V}^T \quad (8)$$

where $\mathbf{U}$ and $\mathbf{V}$ are the (N_d x N_p) and (N_p x N_p) column orthonormal matrices for the data space and parameter space respectively, i.e. $\mathbf{U}^T\mathbf{U} = \mathbf{I}$ and $\mathbf{V}^T\mathbf{V} = \mathbf{I}$, and $\boldsymbol{\lambda}$ is the (N_p x N_p) diagonal matrix of singular values $\lambda_j[1{:}N_p]$. In terms of the singular value decomposition of the scaled and weighted Jacobian or sensitivity matrix $\mathbf{A_s}$, the solution vector $\mathbf{x_s}[1{:}N_p]$ of scaled parameter steps is now computed as (Menke, 1989: Meju, 1994)

$$x_{s[i]} = \mathbf{v}_i\,[\mathbf{1}/\boldsymbol{\Lambda_d}]\,\mathbf{U}^T\mathbf{y} \quad \text{for i=1,..,}N_p \quad (9)$$

where $\mathbf{v}_i$ is the i th row vector in the right-side $\mathbf{V}$ matrix and $\boldsymbol{\Lambda_d} = \text{diag}(\Lambda_{d[i]})$ is the diagonal matrix of damping factors $\Lambda_{d[i]}$ for the ridge regression defined as :

$$\Lambda_{d[i]} = \lambda_i / (\lambda_i^2 + \beta_k^2) \quad \text{for i=1,..,}N_p \quad (10)$$

where β_k is the ridge parameter for the k th trial model step and λ_i is the i th singular value.

The symmetrical (N_p x N_p) covariance matrix $\mathbf{C} = C_{ij} = \text{cov}\,[x_i, x_j]$ is calculated using the relation [see Press *et al*, 1992, p.671]

$$C_{ij} = \text{cov}\,[x_i, x_j] = \sum_{k=1}^{N_p} \gamma_k^2\, V_{ik}\, V_{jk} \quad (11)$$

where $\gamma_k = 1/\lambda_k$ for $\lambda_k \neq 0$ and $C_{ij} = C_{ji}$, from which estimates of the variances $\sigma_{m[i]}^2[1{:}N_p]$ are obtainable as the diagonal elements C_{ij} of the covariance matrix $\mathbf{C}$.

As noted previously, the major advantage of singular value decomposition over other matrix inversion or decomposition techniques, is that SVD enables the user to diagnose and rectify

situations where the matrices **A** and $\boldsymbol{\lambda}$ are singular, i.e. when any $\lambda_k = 0$, or from a numerical standpoint, where any $\lambda_k \approx 0$. This latter situation in which $\boldsymbol{\lambda}$ is ill-conditioned may be tested using the inequality

$$\lambda_k < \max(\lambda_k)\, \varepsilon_w \qquad \text{where } \varepsilon_w = N_p\, \varepsilon_m$$

and ε_m is the machine accuracy or zero tolerance which is about 1.18×10^{-7} for positive floating point numbers in standard IEEE representation (Press *et al*, 1993). Therefore in situations where **A** is deemed as ill conditioned, the ridge parameter β should be made sufficiently large so as to ensure that the parameter perturbation in equation (9) remains physically realizable and has not jumped outside the linear range.

HORIZONTAL GRADIENT SURVEYS

Wing tip mounted TMI sensors are being used widely in mineral exploration surveys to take advantage of gradient enhanced gridding algorithms that improve the effective resolution of magnetic surveys (Nelson, 1994, Hardwick, 1999). With the increasing popularity of this data collection method, we wanted to see what additional information could be delivered through the use of joint inversion technology. We chose two examples that would add value at scales less than the line spacing of the survey.

The first example (Figure 1) looks at the problem of determination of azimuth for linear geological features that cut the flight line at a low angle to the direction of the line. Can we distinguish between a dyke cutting a line at 90 degrees from one at 10 degrees? With conventional TMI data this problem cannot be solved.

A simple model for a vertical dyke was used in the test with azimuthal angles ranging from 10 to 90 degrees and a starting depth 100m deeper than the true model. The width of the dyke is 100m and the depth below the sensor is 100m. Each test converged to an RMS residual error (RMSE) of less than 0.1% within 21 to 33 iterations and confirms that the implicit 3D information in the cross-wing gradient can be used to derive the local geological strike direction from a single line. The depth and thickness of the dyke were recovered to better than 1m in all cases.

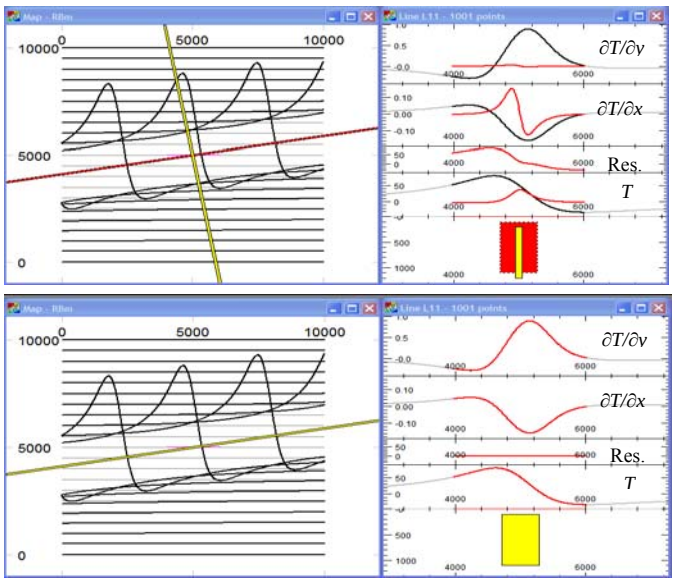

Figure 1: Before (top) and after (bottom) views of the single line joint inversion results for a dyke where the starting azimuth (-10 deg.) is different from the true value (80 deg.) by 90 degrees. The left hand component of each image shows the starting (yellow) and target model (red) and a stacked profile map of the TMI (T) target model response curves. The right hand graph shows the model cross-section, T, TMI residual (Res.), ∂T/∂x and ∂T/∂y in order bottom to top.

The further implication of this outcome is the ability for cross-wing gradient measurements to provide automated strike correction for depth estimation. That is, the depth and azimuth of a dyke can be estimated from a single profile. Thickness and magnetic susceptibility can also be recovered where the thickness is greater than the depth below sensor.

The second example is significant for diamond exploration and is designed to detect the location of a vertical pipe-like intrusion that is offset from the flight line. In this synthetic test we placed a 200m diameter vertical pipe midway between flight lines spaced at 500m with a depth of 100m below the sensor. We then placed a starting model 250m to the east with a starting depth of 200m and diameter of 140m.

The starting model and results of the inversion are shown in Figure 2 in the same manner as the previous dyke test. The line segment used in the modelling is highlighted in red and straddles the TMI low in the stacked profile map. The inversion results produced an x,y location match of less than 1m from the true location, depth match within 3m and radius match within 11m. At an offset of 250m and depth of 100m, we did not expect to resolve the diameter of the pipe as the true diameter is less than the distance from the sensor. An inversion with TMI data would require at least two lines of data to recover the location of the intrusion, yet the joint inversion can recover the location and approximate dimensions by using the horizontal gradient derived from two wingtip TMI sensors.

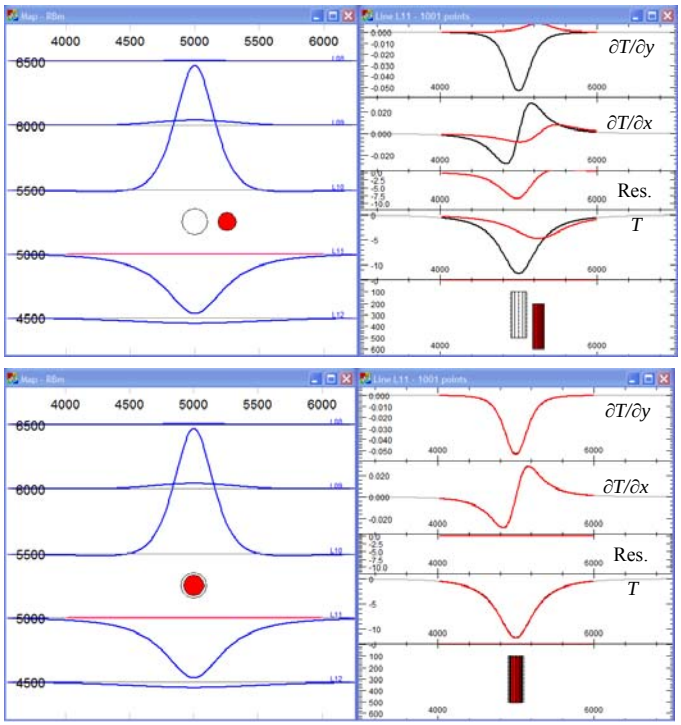

Figure 2: Before (top) and after (bottom) views of the single line joint inversion results for an intrusive pipe model where the starting model (red) is offset 250m to the east. The left hand component of each image shows the model and a stacked profile map of the TMI target model response curves. The right hand graph shows the cross-section, TMI (T), TMI residual (Res.), ∂T/∂x and ∂T/∂y in order bottom to top.

We ran additional tests by offsetting the same starting model 250m north, west and south with equivalent results for the first two, but a failure in the southern offset which diverged in a southerly direction. The starting position for the failed model is directly under the line where the TMI is at a minimum. The RMS error or mismatch for the failed model was very large and thus there is no ambiguity in searching for a better solution by using a different starting location.

We applied the joint inversion method to a horizontal gradient, Midas survey flown over the Groblersdal Platinum Mine near Potgietersrus, South Africa. The helicopter survey was flown at 20m terrain clearance and 50m line spacing so it imaged the near surface geology very effectively. We took one line over a dyke from the survey (Figure 3) to see if we could reproduce the dyke trend directions mapped by the high resolution survey. The inline and cross-wing components of the horizontal gradient vector were transformed into the Cartesian vector components ∂T/∂x and ∂T/∂y.

The TMI data required a DC offset to adjust for the regional whereas the horizontal gradients required no regional adjustment. The joint inversion of all three channels is shown in Figure 4 where a good match is produced for all three.

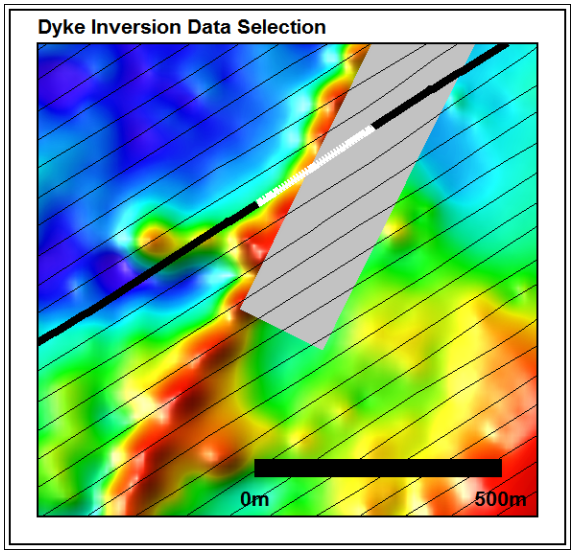

Figure 3. Flight path map and magnetic image showing the model line, data segment and image from a section of the Midas magnetic gradiometer survey. The data selection covers part of the magnetic anomaly produced by a north, north east trending dyke. The gray rectangular zone is the projection of the inverted dipping dyke model onto the map view.

There was a small phase lag between the gradient channels and TMI and we found that the TMI provided no additional geological information over inversion of the horizontal gradients.

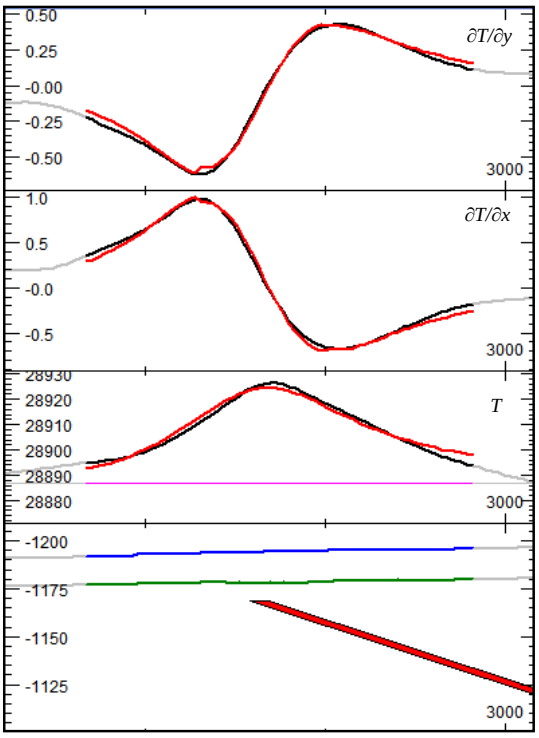

Figure 4. Joint inversion of a dyke model for the single line magnetic data segment shown in Figure 3 using the T, ∂T/∂x and ∂T/∂y data channels (bottom to top). The black curves represent the data channels and red the inversion model channels. In the cross-section view, the blue line shows the sensor elevation and green the ground surface.

TMI AND VERTICAL DERIVATIVE

The first vertical derivative ($\partial T/\partial z$) of the total magnetic field produces excellent results for depth and the location of the upper edges of the magnetic source, whereas the total magnetic intensity provides more information on depth extent. The vertical derivative also contains more implicit 3D information about geological features that are offset from the line (Foss, 2001).

Unfortunately $\partial T/\partial z$ measurements are typically very noisy due to limited separation of the sensors. As a consequence, only a small proportion of surveys are flown with this type of instrument. We can however derive $\partial T/\partial z$ through FFT transformation of the measured TMI grid T_m. We have to assume that the survey is reasonably flat, but the derivative grid can be resampled back onto the original flight lines to provide an additional channel for joint inversion.

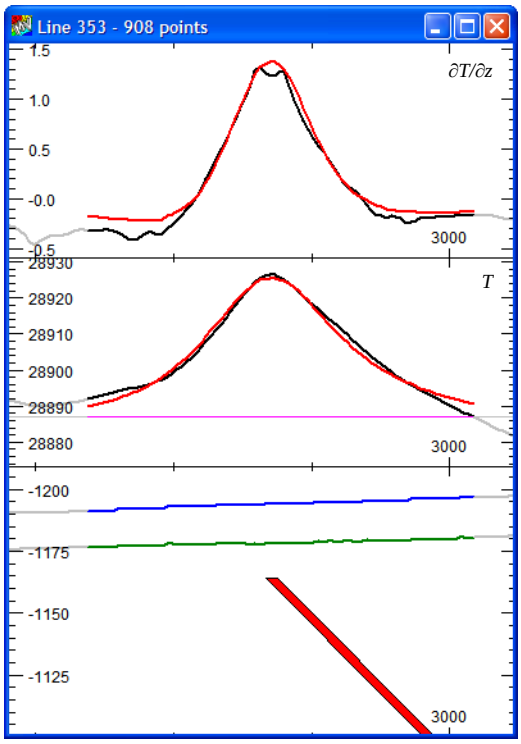

Figure 5. Example of joint inversion of the FFT derived first vertical derivative (top track) with measured total magnetic intensity T(middle track) for the same dyke anomaly used for the horizontal gradient inversion that is illustrated in Figure 4. The measured data are presented in black and inversion model data in red.

We applied the technique to the same line that we used for the horizontal gradient test. The results for this line are shown in Figure 5 where a reasonable match was achieved for both channels. In practise, we found that the method was compromised by the partial filtering influence of the gridding process and subsequent derivation of the first vertical derivative using the FFT process. The apparent upward continuation of the data was of the order 25 – 50% of the grid cell spacing. Also, the first vertical derivative provides no additional information on the azimuth of the dyke.

While the method has promise where the vertical gradient is measured, the additional information provided through grid based calculation does not appear to offer significant

advantages over direct inversion of TMI data for a single line. We expect the additional channel will improve inversion quality when multiple lines are used.

FULL TENSOR MAGNETIC GRADIOMETERS

Full tensor magnetic gradiometers offer the promise of six channels of oriented information delivering B_{xx}, B_{xy}, B_{xz}, B_{yy}, B_{yz}, B_{zz} channels where the notation for element B_{xy} refers to the gradient of the B_x magnetic field component in the y direction ,i.e. $B_{xy} = \partial B_x/\partial y$ and so forth. We also note that the magnetic gradient tensor is a second order symmetric tensor, i.e. $B_{ij} = B_{ji}$ for i,j = x,y,z and that individual tensor elements are harmonic potential field functions (Blakely, 1995). This necessarily implies that the magnetic field vector **B** is the gradient of a scalar magnetic potential Φ and hence satisfies Laplace's equation i.e. for **B** = grad Φ and also div **B** = 0 so that div grad $\Phi = 0$. Hence the trace of the magnetic gradient tensor is identically zero so that $B_{xx} + B_{yy} + B_{zz} = 0$ which implies that there are five independent channels since at least one of the diagonal elements is redundant if the other two are known , for example, $B_{zz} = -(B_{xx} + B_{yy})$. The tensor is measuring the curvature of the potential which contrasts with the scalar measurement of the total field (TMI) and thus provides the vector information that can be used by the joint inversion. Ultimately we expect the tensor to provide significantly more information regarding magnetization direction and higher precision for locating geological boundaries. The B_{zz} component has a large advantage over a FFT derived $\partial T/\partial z$ which generally assumes that the survey was acquired over flat terrain.

We increased the complexity of the pipe model shown in Figure 2 by adding an azimuth and ellipticity to the plan shape of the body as well as an offset from the line (Figure 6). The joint inversion results show that it is possible to recover the pipe radii as well as the centre location and depth. Unlike total field data, we are able to recover the body parameters from a relatively small subset of the data over an anomaly.

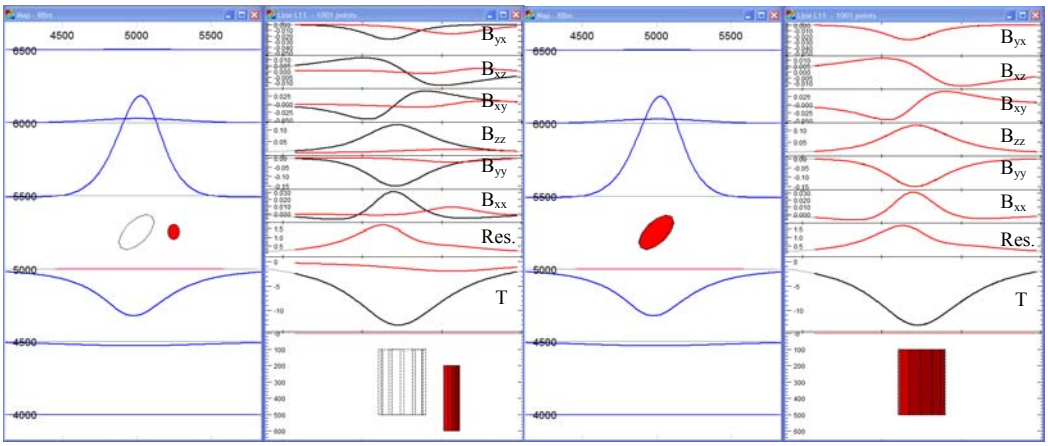

Figure 6. Joint inversion of the full tensor model response from an elliptic pipe that is offset 250m to the north of the inversion data segment. The stacked profile map (a) shows the starting position for the seed model (red) and the cross-section view (b) shows the depth position of the seed model. The stacked profile map (c) shows the final inversion result after 51 iterations and the cross-section view (d) shows the match for TMI and all tensor channels to an RMS mismatch of less than 1%.

We repeated the offset test that failed for the horizontal gradient inversion (250m south offset) and found that the joint inversion could recover the elliptic pipe position by using the full tensor data.

We repeated the tests multiple times using small line segments and even with seven data samples the inversion converged on a satisfactory solution. The built in redundancy of the full

tensor data increases the robustness of the inversion and allows us to reduce the impact of interference from adjacent magnetic sources.

We applied the joint inversion method to a full tensor survey flown over the Groblersdal Platinum Mine near Potgietersrus, South Africa. The helicopter survey was flown with a towed bird at 40m terrain clearance and 100m line spacing over a subset of the area covered by the Midas survey. This survey is significant because it is the first commercial survey flown by Anglo Platinum using a liquid helium cooled sensor developed by IPHT, Jena, Germany. Anglo American, Anglo Platinum and De Beers have been working with IPHT to develop a practical solution for the ultimate high resolution 3D measurement of the magnetic field tensor. Our development of a joint inversion solution for the magnetic tensor was stimulated by this project.

We found an elliptical shaped B_{zz} anomaly extending over three lines of data and used this as a test to see how little field data was required to establish the location and shape of the magnetic source. Images of covering the six tensor channels from a subset of the survey are shown in Figure 7.

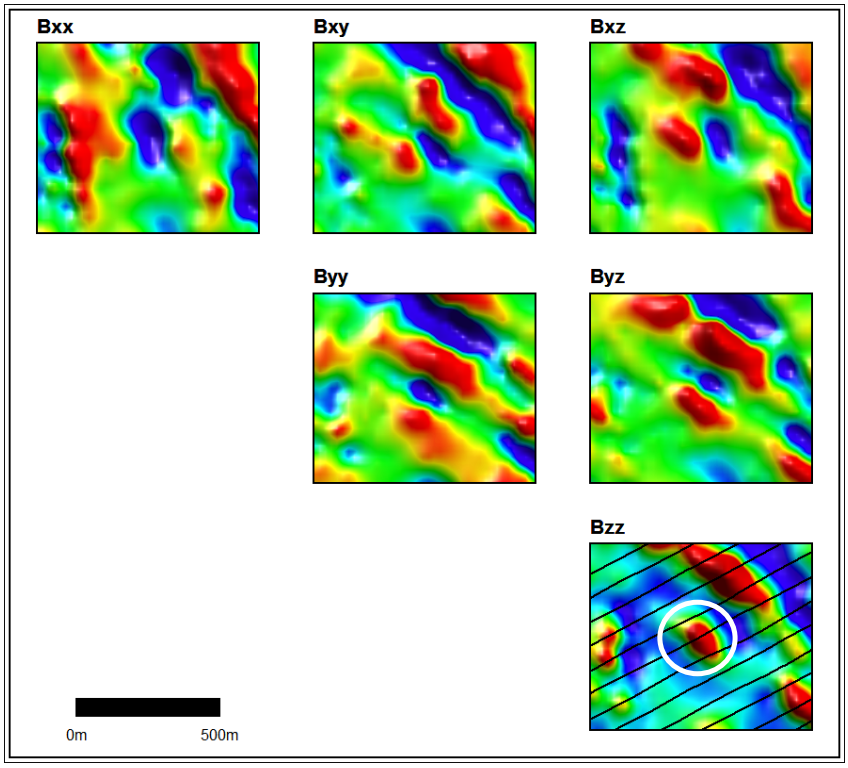

Figure 7. Images of the six tensor channels from a subset of the Potgietersrus survey illustrate the complex nature of the tensor data. The white circle in the bottom right image shows the location of the test anomaly and flight lines.

Segments of data from three adjacent lines were used to model and then invert the tensor data as shown in Figure 8. A starting model of a circular pipe quickly converged to produce an elliptical pipe that straddled two lines and almost reached the third. We also confirmed the results from our theoretical model tests that you only need part of the anomaly data to produce a useful inversion result. In this way it is possible to minimise the influence of interference from adjacent magnetic anomalies. The anomaly is also reversed from the current field direction so we assumed that source is remanently magnetized with a remanent field direction opposite to the earth's present field direction.

We applied the same inversion process sequentially to the individual data segments for each of the three lines to see if we could reproduce the results that we achieved with theoretical models (Figure 6). A successful inversion was produced from each test and the resulting elliptical pipes superimposed in a 3D view (Figure 9). The models are colour coded for Line 11610 (north west) in yellow, Line 11600 (centre) in blue, Line 11590 (south east) in green and the three line segment inversion model in red.

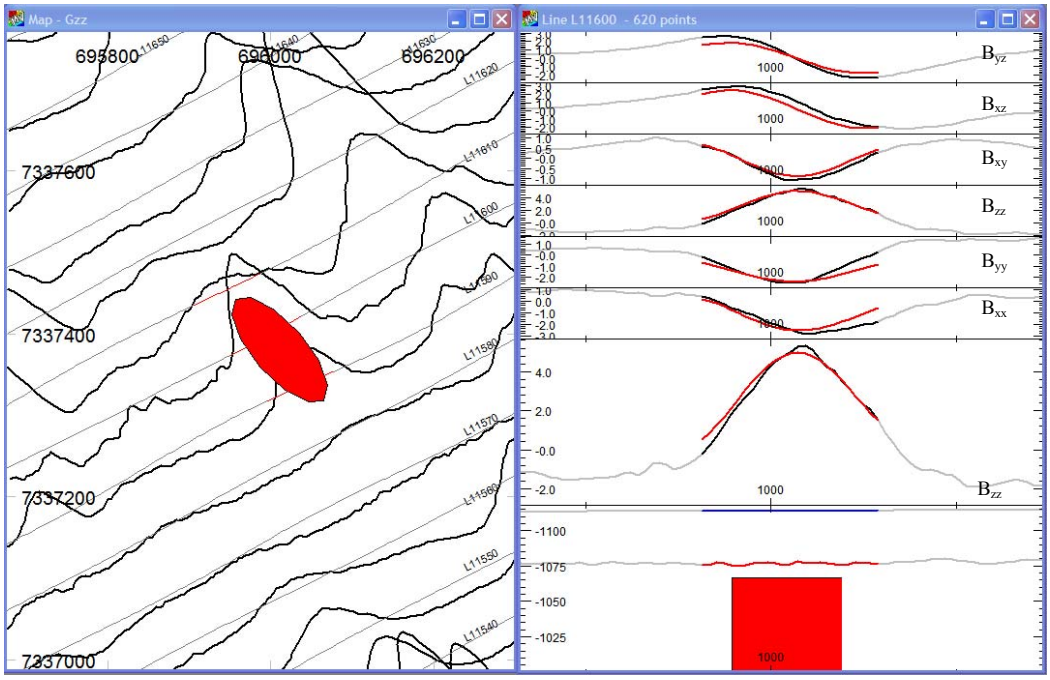

Figure 8. Stacked profile map (left) and cross-section view (right) of the joint inversion result using data segments from three adjacent lines. The centre line (11600) profile section shows the six tensor channels in the upper six tracks and the B_{zz} reference track is duplicated above the cross-section.

The blue centre line (11600) model result is almost identical to the result achieved from all three lines and the green south-east line (11590) model has a close match in dimensions and azimuth. The yellow north-west line (11610) model result has similar dimensions to the other models but the azimuth deviates significantly from the other three models. In this case, the anomaly is believed to be a compound anomaly with a contribution of additional magnetic material immediately to the north west of the line.

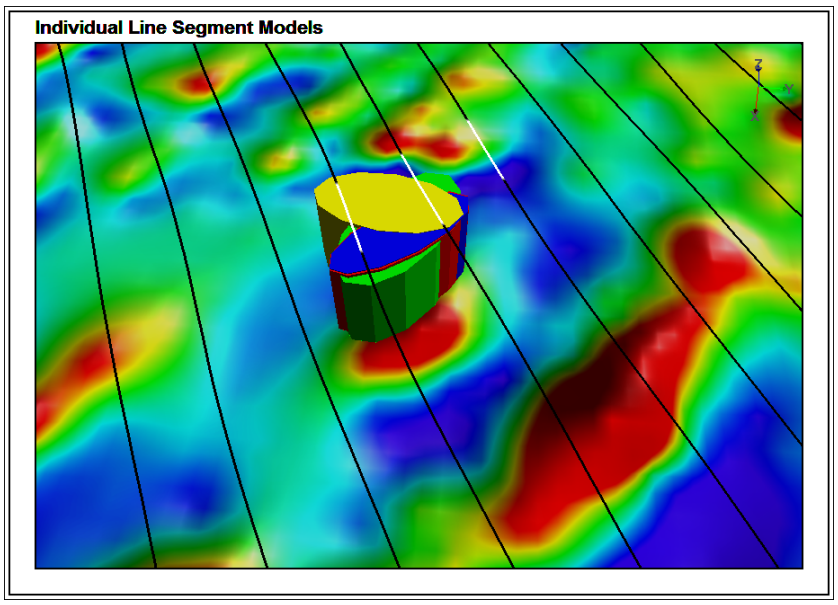

Figure 9. 3D view of the three models derived by joint inversion of individual line segments (green, blue, yellow) and a model derived from all three lines covering the target anomaly (red). The 3D flight path has white highlights to indicate the data regions used for the joint inversion.

SUMMARY AND CONCLUSIONS

We have developed a multi-channel joint inversion algorithm that is well suited to potential field data and tested the method against theoretical forward models and field data. The method is suitable for virtually any instrument combination including multi-sensor total field systems, multi-sensor fluxgate systems, the new generation of SQUID magnetometer systems and full tensor gravity systems.

Joint inversion of multi-channel magnetic data provides improved resolution of geology, particularly where horizontal gradients are measured to sense the presence of magnetic rocks that are not immediately beneath the flight lines. In the case of the cross-wing and full tensor SQUID magnetometers, images of $\partial T/\partial x$, $\partial T/\partial x$, B_{xy}, B_{xx}, etc. are impractical to use as analogues of geology. The total magnetic intensity (T) and B_{zz} measurements are the only practical channels to use for qualitative interpretation. Joint inversion is necessary to extract the additional geological information that is present in these complex data channels.

Cross-wing horizontal total field magnetic gradiometers are in widespread use for producing improved total magnetic field maps, but to our knowledge, little has been done with respect to direct interpretation of the gradient data. We have demonstrated that the horizontal gradient information can have a significant impact on the estimation of geological strike directions, depths and magnetic susceptibility. Gradiometers and full tensor SQUID systems should be used routinely in surveys with wide line spacing such as petroleum surveys and reconnaissance surveys where inversion can help resolve geological detail that is offset from the flight line.

Joint inversion now provides an opportunity to look at historical horizontal gradiometer surveys in new ways with the possibility of extracting new geological information that could be relevant to exploration objectives.

ACKNOWLEDGEMENTS

The authors wish to thank Anglo Platinum, Anglo American and De Beers for their support for the concept and development of algorithms for using joint inversion to extract detailed geological information from full tensor magnetic data. We also thank Anglo Platinum for permission to use and publish data from the Fugro, Midas horizontal gradiometer and IPHT, full tensor SQUID magnetometer surveys.

The authors used Encom ModelVision Pro to perform the joint inversion research and Encom PA Explorer for visualisation and interpretation of the results. We would also like to acknowledge our co-workers Tony White, Clive Foss and Wayne Stasinowsky for their contributions to the development of the joint inversion algorithms and evaluation of experimental results.

REFERENCES

Blakely, R.J., 1995. *Potential Theory in Gravity and Magnetic Applications*, Cambridge University Press, Cambridge and New York, 441pp.

Foss, C.A., 2001. Joint interpretation of gravity and gravity gradient profiles. SEG Expanded Abstracts 20, p.1489, SEG 2001 Annual Meeting.

Hardwick, C.D., 1999, Gradient-enhanced total field gridding, 69th Ann. Internat. Mtg: Soc. of Expl. Geophys.,381-384.

Menke, W., 1989. *Geophysical Data Analysis : Discrete Inverse Theory*, Academic Press, San Diego, 289 pp.

Meju, M.A., 1994. Geophysical Data Analysis: Understanding Inverse Problem Theory and Practice, Course Notes Series, Volume 6, S.N. Domenico (Ed.), Society of Exploration Geophysicists, Tulsa, Oklahoma, 296 pp.

Nelson, J.B., 1994. Levelling total-field aeromagnetic data with measured horizontal gradients, *Geophysics* 59, 1166-1170.

Press, W.H., Teukolsky, S.A., Vetterling, W.T. and Flannery, B.P., 1992. *Numerical recipes in Fortran - The Art of Scientific Computing*, 2nd edition, Cambridge University Press, Cambridge, 963 pp.